Instrument Science Report WFC3 2014-02

The Impact of x-CTE in the WFC3/UVIS detector on Astrometry

Jay Anderson
April 4, 2014

ABSTRACT

Recent observations of the center of globular cluster Omega Centauri are used to estimate the impact of imperfect serial CTE (charge-transfer efficiency) on astrometry in the x coordinate. As of early 2013, after about 4 years in orbit, the horizontal positions of bright stars are affected at the 0.0015-pixel level, and fainter stars are affected at the 0.004-pixel level.

1. Introduction

The impact of imperfect CTE (charge-transfer efficiency) in the parallel direction on the *y*-positions of stars has been well established for ACS/WFC (see Kozhurina-Platais et al. 2009 and Anderson & Bedin 2010), and it has been observed for WFC3/UVIS as well. The pixel-based corrections do a reasonable job correcting for this effect in both cameras. Serial-CTE in ACS was demonstrated in Anderson & Bedin (2010, see Figure 15), however they did not include the serial transfer in their CTE model since at the time there was an ambiguity between serial CTE and the bias-shift effect (which is related to a hysteresis in the readout electronics).

The WFC3 instrument team is working on improving the pixel-based model of Y-CTE currently available for the UVIS detector (http://www.stsci.edu/hst/wfc3/tools/cte_tools). The plan is to include serial-CTE in the model as well, however it would be useful for several astrometric projects currently underway to obtain a rough estimate of its impact on astrometry. Therefore, we conduct a brief study here in an effort to empirically determine its impact.

2. The Astrometric Signature of serial-CTE

Figure 1 shows the readout scheme for the WFC3/UVIS detector. The charge from pixels is shifted in parallel vertically down the chip to the serial register, and then each row is shuffled horizontally to the four different readout amplifiers. This horizontal readout shift is leftward for amplifiers A and C, and rightward for amplifiers B and C.

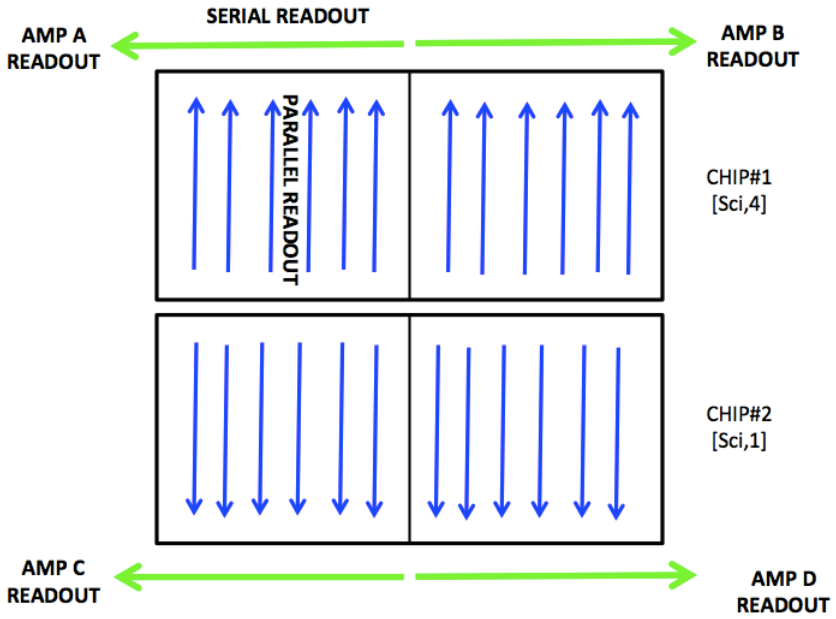

Figure 1: Readout directions for WFC3/UVIS's four amplifiers.

Radiation damage causes charge traps to form in the silicon lattice of the detector. These traps can detain and then release electrons during readout and thus cause the profiles of stars to be blurred in the anti-readout direction. This blurring is a non-linear function of the amount of charge in each pixel, and as such it impacts faint stars more severely than bright ones. The amount of blurring is also a function of the distribution of charge in the preceding pixels.

It is well known that these charge traps form in the chip itself, leading to CTE trails in the vertical direction during the parallel shift. But traps also form in the readout register, leading to trails in the horizontal direction. The horizontal shifting is more than two thousand times faster than the vertical shifting, so the trapping and release time for the serial-CTE is very different than that for parallel-CTE.

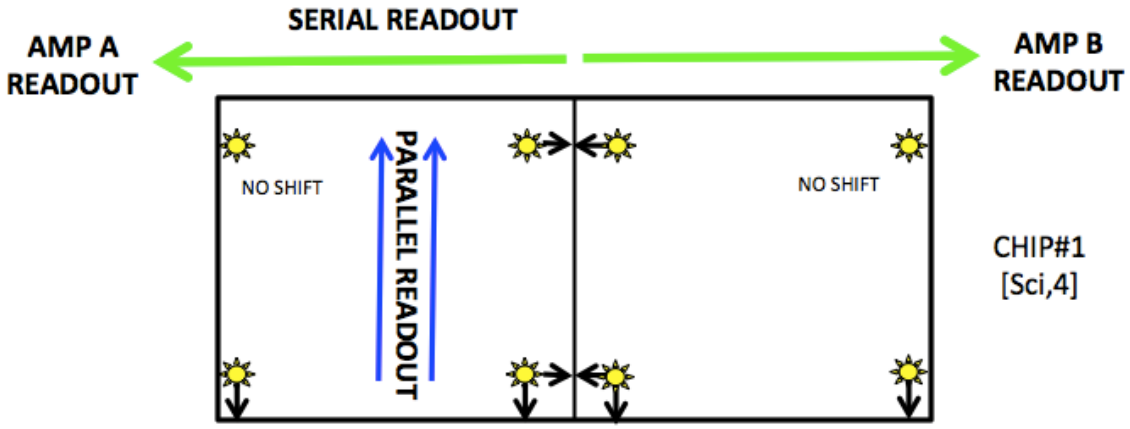

Figure 2: Expected direction for CTE-related astrometric shifts.

3. Observations

The astrometric signature of imperfect CTE is that stars are measured to be farther away from the readout amplifier than they otherwise would be. As a result of the different horizontal-shift directions, stars that lie on opposite sides of the boundary between amplifiers are shuffled in opposite directions and would thus be expected to exhibit opposite astrometric shifts. This makes it particularly easy to examine the impact of x-CTE. The black arrows in Figure 2 show a schematic of what one might expect imperfect CTE to do to positions, both in the *x* and in *y* directions.

To investigate the CTE-related *x* shift, we evaluate eight F606W observations of globular cluster Omega Cen taken for program CAL-13100 (PI-Kozhurina-Platais) for the purposes of distortion calibration. Table 1 below summarizes the details of the data set. These eight exposures were acquired at orientations differing by ~10 degrees and/or dithers differing by 1000 pixels, such that stars that are close to the inter-amplifier boundary in one observation are far from it in the others. We chose images that were collected close in time so that the internal proper motions of the stars (1 mas/year = 0.02 pixel/year) will not have a significant impact on our results.

Table 1. Summary of observations.

#	NAME	OBS-DATE	POS-TARG	PA_V3	EXPTIME
1	ic4j02hdq	02 feb 2013	(0,0)	129.9	48s
2	ic4j02hgq	02 feb 2013	(-40,40)	129.9	48s
3	ic4j02hjq	02 feb 2013	(40,-40)	129.9	48s
4	ic4j03jbq	24 mar 2013	(0,0)	174.9	48s
5	ic4j03jeq	24 mar 2013	(-40,40)	174.9	48s
6	ic4j04zhq	14 mar 2013	(0,0)	136.0	40s
7	ic4j05zjq	14 mar 2013	(0,0)	151.0	40s
8	ic4j06zlq	14 mar 2013	(0,0)	166.0	40s

4. Reductions

We ran the publicly available software routine `img2xym_wfc3uv` (written by J.A.[1]), along with empirically determined library PSFs (as described in Bellini et al 2011, B11), to find and measure all the reasonably bright stars in each of the exposures[2]. (It is worth noting that the PSFs used here are continuous across the amplifier boundary, since the chip is continuous across the boundary.)

The typical exposure had 150,000 identifiable stars. We applied the distortion solution from B11 to each star position. Next we collated all the exposures into the distortion-corrected reference frame of the first exposure and made a list of all stars that were found in a minimum of four exposures. We then cross-matched this star list with the lists from each exposure and recorded the raw and distortion-corrected positions for each star in each exposure.

5. Analysis

The next step was to examine the horizontal shift between amplifiers. To do this we went through each exposure and identified every star that was within 75 pixels of the inter-amplifier boundary ($i>1972$ and $i<2124$). For each of these stars, we also identified all the relatively bright (S/N >75) neighboring stars that were: (1) in the same WFC3/UVIS chip, (2) within ±75 pixels in y of the star's raw position, and (3) also within ±75 pixels of the inter-amplifier boundary. The top half of Figure 3 shows this selection. There were typically 50 or so such reference stars.

We next went through the seven other exposures and determined whether the target star and 90% of the reference stars could be found and were all in same amplifier. The bottom half of Figure 3 shows a typical case for setup of the comparison exposure.

The goal was to use the comparison exposure to estimate the true positions of the stars, so that we could determine whether the amplifier boundary introduces any offset between them. To do this, we took the positions of the reference stars in the two frames to define a transformation from distortion-corrected frame of the comparison exposure into the distortion-corrected frame of the first exposure. This transformation was restricted to have only translation and rotation (3 parameters). We assumed that over

[1] The program is available at the following location:
http://www.stsci.edu/~jayander/WFC3/WFC3UV_PSFs/img2xym_wfc3uv.F.

[2] Finding parameters HMIN=5 and FMIN=50 and PMAX=64999 were used, which means that in order to be found, the brightest pixel of a star had to have no brighter pixels within a radius of 5.5 pixels, the flux in the central 3x3 pixels had to be at least 50 electrons over sky, and the brightest pixel could not be saturated. This brightness limit corresponds to an instrumental magnitude of about −5.5.

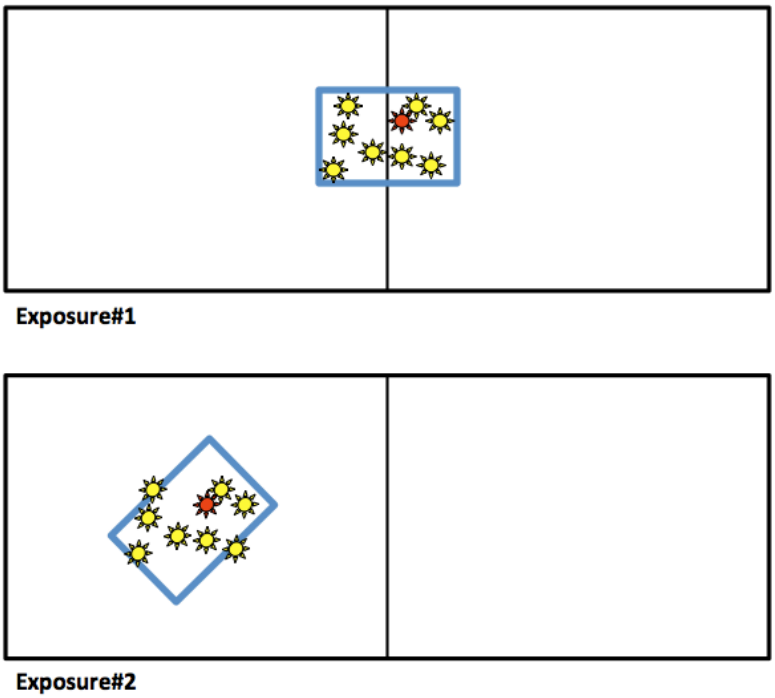

Figure 3: The top figure shows the selection of a target star and its reference stars, and the bottom half shows the same stars in the comparison image. The red star is the target star and the yellow stars are the reference stars.

such a small distance (150 pixels) any variation of scale due, perhaps, to breathing or velocity aberration, would be negligible.

We used this transformation to estimate the true position of the target star in the first exposure, so that we could compare it against the observed position. We were able to identify about 144,000 such comparisons between a target star in one exposure and a comparison exposure, for target stars between a S/N of 30 and saturation (S/N ~ 500).

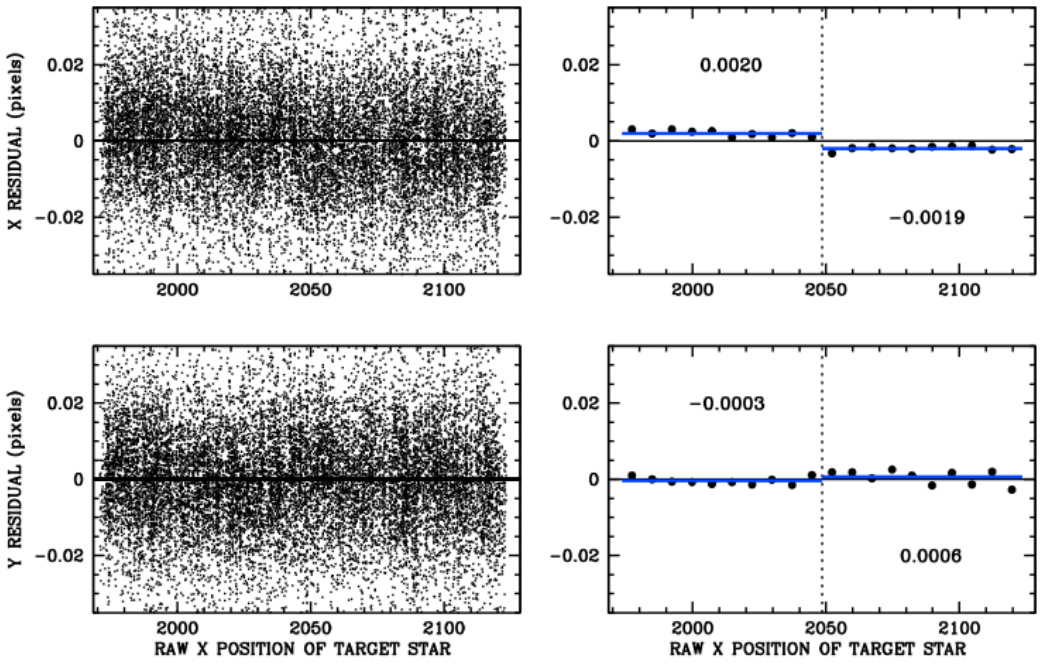

Figure 4: On the left, we show in the top (and bottom) panels the x (and y) residuals for stars with instrumental magnitudes between -11.5 and -12.5 (S/N ~ 250). Each point corresponds to a bright star observed to be near the amplifier boundary in one exposure. On the right, we distill these residuals into bins that are 7.5-pixels wide, and also report the average for the left and right amplifiers. The fact that we see a shift in x, but not in y is consistent with x-CTE.

The next step is to look for trends. Figure 4 shows the raw residuals for stars with S/N of ~ 250. We show the residuals in both *x* and *y*, so that y can act as a control sample. The typical residual is ~0.01 pixel (0.4 mas), indicative of the measurement error of a bright star in a single exposure and the quality of the distortion solution (see B11).

In the right panels, we bin the sigma-clipped residuals into ten 7.5-pixel-wide bins for each half of the chip. It is clear that in the upper plot, the *x* residuals tend to be slightly positive in the left half of the chip and slightly negative in the right half of the chip. The amplitude of the shift from zero is roughly ±0.002 pixel. The *y* residuals do not show any significant trend with respect to the amplifier boundary.

Figure 4 shows the results for only the bright stars with S/N ~ 250. In Figure 5 on the next page, we show the results for all stars, from S/N ~ 500 to S/N ~ 35. The offset increases systematically from 0.0015 pixel at the bright end to 0.004 pixel at the faint end. The crowding makes it difficult to study the trends for even fainter stars.

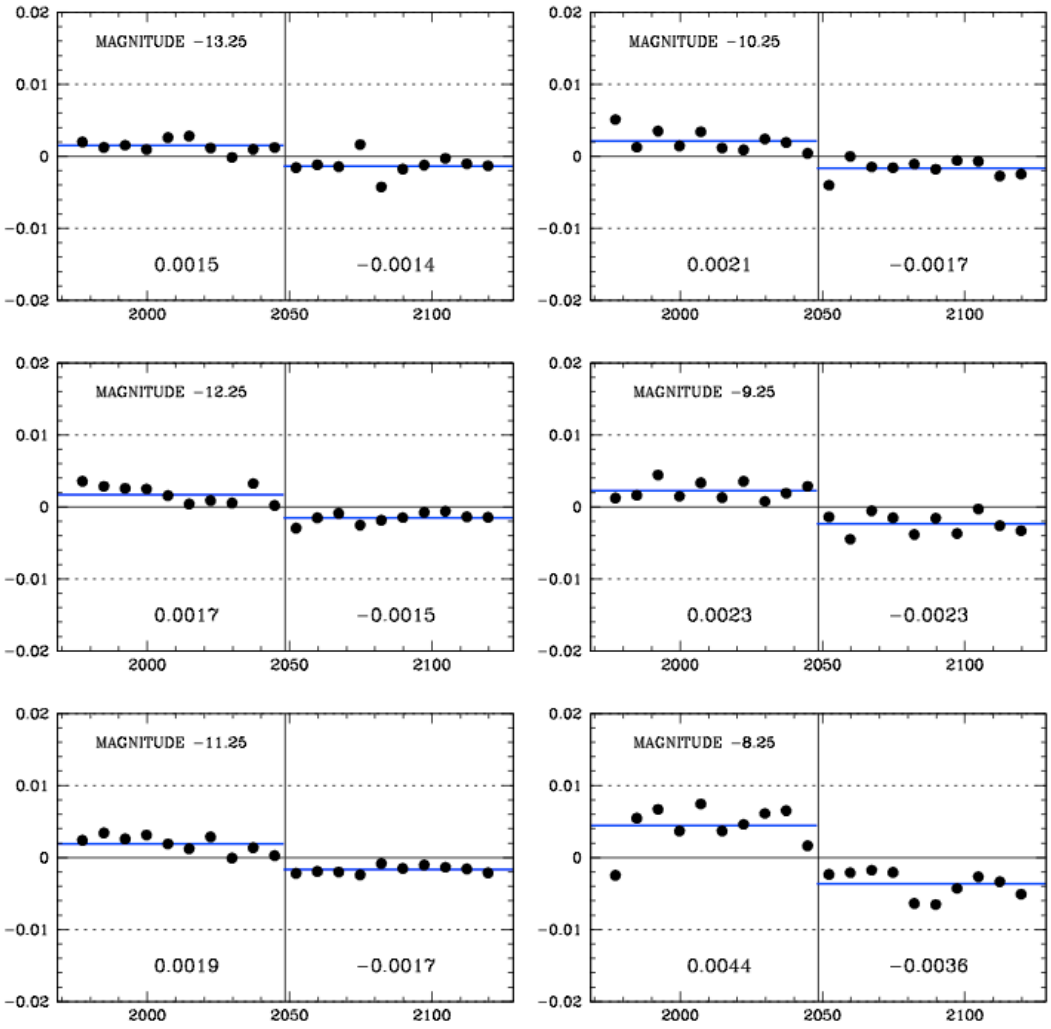

Figure 5: Binned residuals and averages for the target star as a function of instrumental magnitude. The brightest bin corresponds to the stars just below saturation.

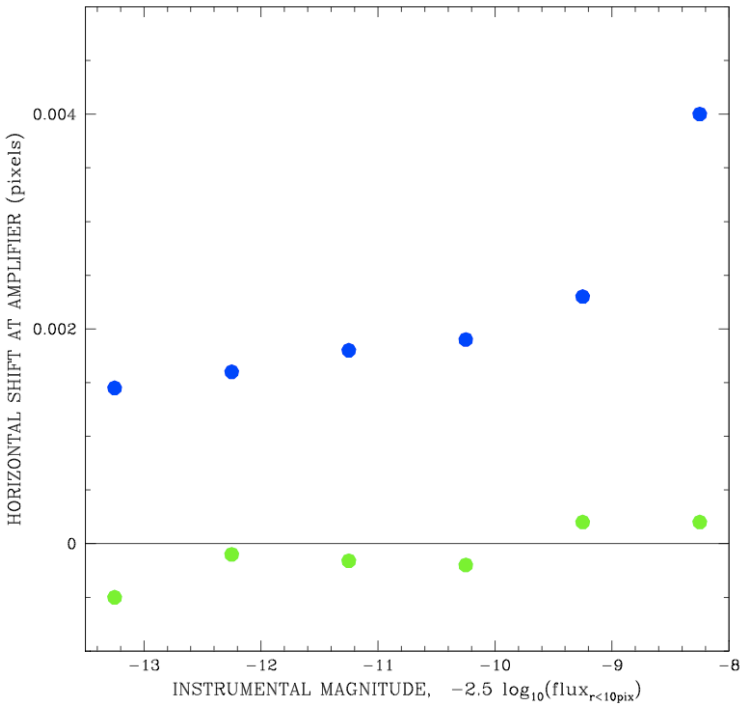

Figure 6: The blue points show the trend of the horizontal shift corresponding to 2048 horizontal serial shifts as a function of instrumental magnitude for the early-2013 data. The background in the typical exposure is about 40 electrons. The green points show the trend for 2010, soon after installation, when radiation damage was minimal.

The blue points in Figure 6 show the overall trend with magnitude in the early 2013 data. The post-SM4 ACS readout electronics exhibit a small amount of readout hysteresis, such that a pixel read out first has a small influence on subsequent pixels (see ACS/ISR-2012-02 by Golimowski et al. on the "bias-shift" correction). The ACS readout hysteresis effect can resemble x-CTE, except that it should be independent of magnitude. The trend with magnitude seen in the WFC3 results shown in Figure 6 would seem to suggest the presence of at least some level of imperfect x-CTE.

In an effort to determine how much of the trend in WFC3 is related to x-CTE, we performed the same experiment on a similar set of exposures of the same cluster that were taken very soon after SM4, when the WFC3/UVIS CTE should have been nearly perfect. The green points in Figure 6 show that there was no net horizontal offset present in the early data, further bolstering the CTE interpretation.

6. Conclusions and Further Work

It is clear from this study that horizontal CTE losses introduce a small but measurable astrometric shift. As of early 2013, when WFC3/UVIS had been in orbit for about 4 years, the shift was about 0.0015 pixel for bright stars, and 0.004 pixel for faint stars in images that had backgrounds of about 40 electrons. No strong signature was seen in early data, so it appears that these shifts are indeed related to x-CTE.

It is not clear what the photometric effect of x-CTE losses will be. Cursory analysis of the horizontal-overscan region indicates that the traps that generate these CTE losses are extremely fast and appear to deposit almost all of the trapped charge in the first pixel of the trail, but we have yet not done a quantitative study to determine whether there may also be some longer-lived traps as well.

The WFC3/UVIS team is planning to recalibrate the pixel-based y-CTE correction in Spring 2014. At that time, we will also examine the feasibility of extending the CTE correction to include the x-component and study the astrometric trend for fainter stars to determine whether they suffer more than 0.004-pixel shifts. Stay tuned.

References

Kozhurina-Platais, V. et al. "Differential CTE Corrections for Astrometry and Photometry for Non-Drizzled Images" ACS/ISR-07-04

Anderson, J. & Bedin, L. R. "An Empirical Pixel-Based Correction for Imperfect CTE. I. HST's Advanced Camera for Surveys" 2010 PASP 122 1034

Bellini, A., Anderson, J. & Bedin, L. R. "Astrometry and Photometry with HST WFC3. II Improved Geometric-Distortion Corrections for 10 Filters of the UVIS Channel" 2011 PASP 123 622